INTERFACIAL CRACK ANALYSIS IN LAYERED MEDIA USING COUPLE-STRESS ELASTICITY AND THE DISPLACEMENT DISCONTINUITY METHOD

Sok An Yin, Jintara Lawongkerd*

Thammasat University, Pathumthani, 12120, Thailand

*Corresponding author: ljintara@engr.tu.ac.th

(Received: March 31, 2026; Revised: May 15, 2026; Accepted: June 05, 2026)

DOI: 10.31130/ud-jst.2026.24(7B).585E

Abstract - Interfacial cracks between dissimilar materials represent a critical failure mechanism in layered structural systems such as coatings, composite laminates, and micro-structured materials. However, classical elasticity theory cannot adequately capture the size-dependent behavior observed at micro- and nano-scales. This study investigates a pre-existing interfacial crack in a multilayered elastic medium using couple-stress elasticity and the displacement discontinuity method. The crack is modeled as a prescribed normal opening displacement discontinuity along the interface between two bonded layers resting on an elastic half-plane. The corresponding reaction tractions, stress fields, and couple-stress components are determined using Fourier transform techniques and Gauss-Legendre quadrature. The numerical results indicate that the material length-scale parameter and stiffness mismatch significantly influence the near-tip reaction stress field. For a prescribed crack opening, couple-stress effects enhance the microstructural resistance near the crack tip, highlighting the importance of size-dependent modeling in the analysis of layered interfacial fracture problems.

Keywords – Couple-stress theory; Interfacial displacement discontinuity; Layered media; Microstructures; Size-dependent effects

1. Introduction

Layered and multilayered materials are widely used in modern engineering applications, including coatings, composite laminates, and micro-structured systems, because they combine the advantageous properties of different materials and achieve enhanced mechanical performance, improved durability, and greater resistance to environmental effects. However, the presence of material interfaces also introduces potential sites for damage initiation, particularly in the form of interfacial cracks, which can lead to delamination and structural failure. Therefore, accurate prediction of the mechanical response near interfacial cracks is essential to ensure the reliability and safety of layered systems.

Experimental investigation of fracture behavior at small scales remains challenging because of the limited dimensions and complex interactions at material interfaces. Consequently, analytical and numerical methods play an important role in understanding crack behavior in layered media. Classical elasticity theory has been widely used to analyze crack problems; however, it does not incorporate intrinsic material length scales and therefore cannot capture size-dependent effects observed in micro-structured materials. To overcome this limitation, generalized continuum theories, such as couple-stress elasticity, have been developed [1–3]. This theory introduces additional rotational degrees of freedom and a material length-scale parameter, thereby enabling the modeling of microstructural effects on the mechanical response.

Recent studies have applied couple-stress elasticity to fracture problems and demonstrated that couple stresses significantly modify the stress field near crack tips, introducing size-dependent behavior that deviates from the predictions of classical elasticity [4–8]. Wongviboonsin et al. [7] investigated size effects in two-dimensional layered materials and showed that the material length-scale parameter substantially influences the mechanical response. Wongviboonsin et al. [8] subsequently extended the analysis to multilayered substrates, while Wongviboonsin et al. [9] examined an interfacial displacement discontinuity in a coated substrate incorporating couple-stress effects. These studies highlight the importance of incorporating length-scale effects in the analysis of cracks in layered media. However, the extension to a fully multilayered system consisting of multiple bonded layers, together with a displacement-discontinuity crack formulation and a parametric investigation of material mismatch effects, has not been comprehensively addressed in the literature.

For numerical modeling of cracks, the displacement discontinuity method (DDM) is a powerful and efficient approach [4–5]. In this method, the crack is represented by a distribution of displacement discontinuities along the crack line, which generates the corresponding stress and displacement fields in the surrounding medium. The DDM is particularly suitable for interfacial crack problems because it can directly represent discontinuities along material interfaces.

Although previous studies have examined couple-stress effects in layered materials and coated substrates, most available formulations focus on single coating–substrate systems or prescribed traction/dislocation formulations. The displacement-controlled interfacial crack in fully multilayered medium with systematic stiffness mismatch remains insufficiently investigated. The novelty of the present work is threefold: (i) the couple-stress displacement discontinuity formulation is extended from coated-substrate benchmark problems to a multilayered system consisting of two bonded elastic layers resting on an elastic half-plane; (ii) the interfacial crack is modeled through a prescribed opening displacement, such that the computed interfacial tractions represent reaction quantities rather than prescribed external loads; and (iii) the effect of stiffness mismatch is investigated through HHS, SHS, and HSS material configurations. Accordingly, the objective of this study is to develop a numerical framework for the analysis of an interfacial crack in multilayered elastic media using couple-stress elasticity and the displacement discontinuity method. The proposed formulation accounts for material heterogeneity and intrinsic length-scale effects and enables the computation of displacement fields, stress components, and couple-stress components.

2. Problem description

Consider a two-dimensional multilayered elastic system consisting of two perfectly bonded elastic layers, each of thickness h, resting on an elastic half-plane substrate, as shown in Figure 1. A Cartesian coordinate system (x, y) is defined such that the x-axis lies along the top surface of the upper layer ($y = 0$), while the y-axis is directed downward into the medium. The regions are defined as follows: the upper layer (Layer 1) occupies $0 \le y \le h$, the lower layer (Layer 2) occupies $h \le y \le 2h$, and the half-plane substrate occupies $y \ge 2h$.

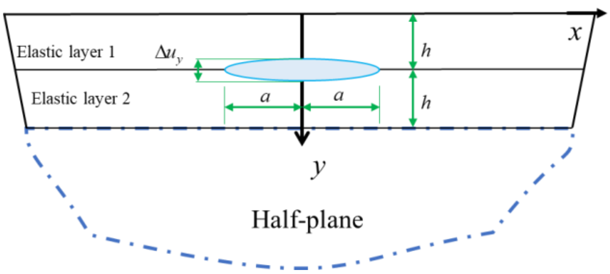

Figure 1. *Geometry and coordinate system of the multilayered elastic medium with an interfacial opening displacement discontinuity of length* $2a$

An interfacial crack is located along the interface between Layer 1 and Layer 2 at $y = h$. The crack extends over a finite length $2a$, and is located along $x \in [-a, a]$. In the present formulation, the crack is modeled using a displacement-controlled approach, in which a prescribed opening displacement discontinuity is imposed along the interface. The displacement jump is defined as $\Delta u_y(x) = u_y(x, h^+) - u_y(x, h^-), x \in [-a, a]$, where h^+ and h^- denote the limiting values approaching the interface from Layer 1 and Layer 2, respectively.

Unlike conventional traction-based formulations, in which tractions are prescribed and displacements are determined, the displacement discontinuity method (DDM) directly prescribes the crack opening displacement. This approach is particularly suitable for modeling cracks as continuous distributions of dislocations and provides improved numerical stability in the presence of stress singularities.

In this formulation, the imposed displacement discontinuity serves as the primary input, while the resulting interfacial tractions, displacement field, stress field, and couple-stress field in the layered medium are obtained as part of the solution. All materials are assumed to be homogeneous, isotropic, and linearly elastic, and their behavior is described by couple-stress elasticity theory [1–3], which incorporates an intrinsic material length-scale parameter ℓ to capture size-dependent mechanical effects.

3. Basic field equations and interface crack formulation

Following the couple-stress theory [1–3], consider a body occupying a domain in the (x, y) plane under plane strain conditions (i.e., $u_x = u_x(x, y)$, $u_y = u_y(x, y)$, $u_z = 0$). The equilibrium equations in the absence of the body force and body couple are expressed as follows:

$$\frac{\partial \sigma_{xx}}{\partial x} + \frac{\partial \sigma_{yx}}{\partial y} = 0 \tag{1a}$$

$$\frac{\partial \sigma_{xy}}{\partial x} + \frac{\partial \sigma_{yy}}{\partial y} = 0 \tag{1b}$$

$$\frac{\partial m_{xz}}{\partial x} + \frac{\partial m_{yz}}{\partial y} + \sigma_{xy} - \sigma_{yx} = 0 \tag{1c}$$

where $\{u_x, u_y\}$ are components of the in-plane displacements, $\{\sigma_{xx}, \sigma_{xy}, \sigma_{yx}, \sigma_{yy}\}$ are the in-plane force stress components, and $\{m_{xz}, m_{yz}\}$ are the non-zero couple stress components. The constitutive relations are given by:

$$\sigma_{xx} = \frac{2\mu}{1-2\nu}\left[(1-\nu)\varepsilon_{xx} + \nu\varepsilon_{yy}\right] \tag{2a}$$

$$\sigma_{yy} = \frac{2\mu}{1-2\nu}\left[\nu\varepsilon_{xx} + (1-\nu)\varepsilon_{yy}\right] \tag{2b}$$

$$\sigma_{xy} = 2\mu\varepsilon_{xy} - 2\mu\ell^2\Delta\omega_z \tag{2c}$$

$$\sigma_{yx} = 2\mu\varepsilon_{xy} + 2\mu\ell^2\Delta\omega_z \tag{2d}$$

$$m_{xz} = 4\eta\frac{\partial \omega_z}{\partial x} \tag{2e}$$

$$m_{yz} = 4\eta\frac{\partial \omega_z}{\partial y} \tag{2f}$$

where $\{\varepsilon_{xx}, \varepsilon_{xy}, \varepsilon_{yx}, \varepsilon_{yy}\}$ are the in-plane strain components; ω_z is non-zero rotation component; Δ denotes the two-dimensional Laplacian operator; μ, ν, and ℓ denote the shear modulus, Poisson's ratio, and the characteristic material length, respectively; and $\eta = \mu\ell^2$. The kinematic relations are given by:

$$\varepsilon_{xx} = \frac{\partial u_x}{\partial x} \tag{3a}$$

$$\varepsilon_{yy} = \frac{\partial u_y}{\partial y} \tag{3b}$$

$$\varepsilon_{xy} = \varepsilon_{yx} = \frac{1}{2}\left(\frac{\partial u_x}{\partial y} + \frac{\partial u_y}{\partial x}\right) \tag{3c}$$

$$\omega_z = \frac{1}{2}\left(\frac{\partial u_y}{\partial x} - \frac{\partial u_x}{\partial y}\right) \tag{3d}$$

Substituting Eq. (3) into Eq. (2) yields the expressions for the force stress and couple-stress components in terms of the displacement field:

$$\sigma_{xx} = \frac{2\mu}{1-2\nu}\left[(1-\nu)\frac{\partial u_x}{\partial x} + \nu\frac{\partial u_y}{\partial y}\right] \tag{4a}$$

$$\sigma_{yy} = \frac{2\mu}{1-2\nu}\left[\nu\frac{\partial u_x}{\partial x} + (1-\nu)\frac{\partial u_y}{\partial y}\right] \tag{4b}$$

$$\sigma_{xy} = \mu\left(\frac{\partial u_x}{\partial y} + \frac{\partial u_y}{\partial x}\right) - \mu\ell^2\left(\frac{\partial^3 u_y}{\partial x^3} - \frac{\partial^3 u_x}{\partial x^2 \partial y} + \frac{\partial^3 u_y}{\partial x \partial y^2} - \frac{\partial^3 u_x}{\partial y^3}\right) \tag{4c}$$

$$\sigma_{yx} = \mu\left(\frac{\partial u_x}{\partial y} + \frac{\partial u_y}{\partial x}\right) + \mu\ell^2\left(\frac{\partial^3 u_y}{\partial x^3} - \frac{\partial^3 u_x}{\partial x^2 \partial y} + \frac{\partial^3 u_y}{\partial x \partial y^2} - \frac{\partial^3 u_x}{\partial y^3}\right) \tag{4d}$$

$$m_{xz} = 2\mu\ell^2\left(\frac{\partial^2 u_y}{\partial x^2} - \frac{\partial^2 u_x}{\partial x \partial y}\right) \tag{4e}$$

$$m_{yz} = 2\mu\ell^2\left(\frac{\partial^2 u_y}{\partial x \partial y} - \frac{\partial^2 u_x}{\partial y^2}\right) \tag{4f}$$

Substituting the constitutive relations in Eq. (4) into the equilibrium equations in Eq. (1) yields a coupled system of fourth-order partial differential equations for the two displacement components u_x and u_y:

$$\frac{2(1-\nu)}{1-2\nu}\frac{\partial^2 u_x}{\partial x^2} + \frac{\partial^2 u_x}{\partial y^2} - \ell^2\frac{\partial^4 u_x}{\partial x^2 \partial y^2} - \ell^2\frac{\partial^4 u_x}{\partial y^4} + \frac{1}{1-2\nu}\frac{\partial^2 u_y}{\partial x \partial y} + \ell^2\frac{\partial^4 u_y}{\partial x^3 \partial y} + \ell^2\frac{\partial^4 u_y}{\partial x \partial y^3} = 0 \tag{5}$$

$$\frac{1}{1-2\nu}\frac{\partial^2 u_x}{\partial x \partial y} + \ell^2\frac{\partial^4 u_x}{\partial x \partial y^3} + \ell^2\frac{\partial^4 u_x}{\partial x^3 \partial y} + \frac{2(1-\nu)}{1-2\nu}\frac{\partial^2 u_y}{\partial y^2} + \frac{\partial^2 u_y}{\partial x^2} - \ell^2\frac{\partial^4 u_y}{\partial x^2 \partial y^2} - \ell^2\frac{\partial^4 u_y}{\partial x^4} = 0 \tag{6}$$

To obtain the solution for a representative elastic layer, the Fourier integral transform is introduced with respect to the horizontal coordinate x. For a function $f(x,y)$ defined in the domain $-\infty < x < \infty$ and $a \le y \le b$, the transform pair is defined as follows [10]:

$$\bar{f}(\xi,y) = \int_{-\infty}^{\infty} f(x,y)\, e^{i\xi x} dx \tag{7}$$

$$f(x,y) = \frac{1}{2\pi}\int_{-\infty}^{\infty} \bar{f}(\xi,y)\, e^{-i\xi x} d\xi \tag{8}$$

where ξ is a transform parameter and $i = \sqrt{-1}$. By applying a Fourier integral transform in Eq. (7) to Eqs. (5) and (6) with respect to the coordinate x, the following system of linear ODEs with respect to the coordinate y:

$$\begin{bmatrix} -\alpha\xi^2 + (1+\ell^2\xi^2)\frac{d^2}{dy^2} - \ell^2\frac{d^4}{dy^4} & -i\xi\left(\beta\frac{d}{dy} - \ell^2\xi^2\frac{d}{dy} + \ell^2\frac{d^3}{dy^3}\right) \\ -i\xi\left(\beta\frac{d}{dy} - \ell^2\xi^2\frac{d}{dy} + \ell^2\frac{d^3}{dy^3}\right) & -\xi^2(1+\ell^2\xi^2) + (\alpha+\ell^2\xi^2)\frac{d^2}{dy^2} \end{bmatrix}\begin{Bmatrix} \bar{u}_x \\ \bar{u}_y \end{Bmatrix} = \begin{Bmatrix} 0 \\ 0 \end{Bmatrix} \tag{9}$$

where $\alpha = 2(1-\nu)/(1-2\nu)$ and $\beta = 1/(1-2\nu)$. The solution of Eq. (9) can be obtained using standard techniques for homogeneous linear equations.

Finally, the general solution for the displacement components in the k-th layer is expressed as follows [7]:

$$\begin{aligned} \bar{u}_x{}^{(k)} = {} & -i|\xi|e^{-|\xi|(h^{(k)}-y^{(k)})}C_1{}^{(k)} - i[\kappa^{(k)} + |\xi|y^{(k)}]e^{-|\xi|(h^{(k)}-y^{(k)})}C_2{}^{(k)} \\ & + i|\xi|e^{-|\xi|y^{(k)}}C_3{}^{(k)} - i[\kappa^{(k)} - |\xi|y^{(k)}]e^{-|\xi|y^{(k)}}C_4{}^{(k)} \\ & - \frac{i\zeta^{(k)}}{\ell^{(k)}}e^{-\zeta^{(k)}(h^{(k)}-y^{(k)})/\ell}C_5{}^{(k)} + \frac{i\zeta^{(k)}}{\ell^{(k)}}e^{-\zeta^{(k)}y^{(k)}/\ell}C_6{}^{(k)} \end{aligned} \tag{10}$$

$$\begin{aligned} \bar{u}_y{}^{(k)} = {} & \xi e^{-|\xi|(h^{(k)}-y^{(k)})}C_1{}^{(k)} + \xi y^{(k)}e^{-|\xi|(h^{(k)}-y^{(k)})}C_2{}^{(k)} \\ & + \xi e^{-|\xi|y^{(k)}}C_3{}^{(k)} + \xi y^{(k)}e^{-|\xi|y^{(k)}}C_4{}^{(k)} \\ & + \xi e^{-\zeta^{(k)}(h^{(k)}-y^{(k)})/\ell}C_5{}^{(k)} + \xi e^{-\zeta^{(k)}y^{(k)}/\ell}C_6{}^{(k)} \end{aligned} \tag{11}$$

where $\kappa = 3-4\nu$, and $C_i(\xi), i = 1,2,3,\dots,6$, are unknown Fourier-domain coefficient functions. The parameter $\zeta = \sqrt{1+\xi^2\ell^2}$ represents the contribution of the intrinsic material length scale within the couple-stress formulation.

Substituting the displacement expressions from Eqs. (10)–(11) into the governing relations of the layered configuration shown in Figure 1 allows the displacement field in each elastic layer and the half-plane substrate to be treated separately. This procedure reduces the governing field equations in each layer to coupled ordinary differential equations with respect to the vertical coordinate y.

By applying the Fourier transform, the displacement, rotation, force-stress, and couple-stress components of the k-th layer are expressed in the following matrix-vector form as:

$$\bar{U}_t^{(1)}\Big|_{y=0} = \begin{Bmatrix} \bar{u}_x^{(t1)} \\ \bar{u}_y^{(t1)} \\ \bar{\omega}_z^{(t1)} \end{Bmatrix}, \bar{U}_b^{(1)}\Big|_{y=h_1} = \begin{Bmatrix} \bar{u}_x^{(b1)} \\ \bar{u}_y^{(b1)} \\ \bar{\omega}_z^{(b1)} \end{Bmatrix} \tag{12}$$

$$\bar{P}_t^{(1)}\Big|_{y=0} = \begin{Bmatrix} \bar{\sigma}_{yx}^{(t1)} \\ \bar{\sigma}_{yy}^{(t1)} \\ \bar{m}_{yz}^{(t1)} \end{Bmatrix}, \bar{P}_b^{(1)}\Big|_{y=h_1} = \begin{Bmatrix} \bar{\sigma}_{yx}^{(b1)} \\ \bar{\sigma}_{yy}^{(b1)} \\ \bar{m}_{yz}^{(b1)} \end{Bmatrix} \tag{13}$$

$$\bar{U}_t^{(2)}\Big|_{y=h_1} = \begin{Bmatrix} \bar{u}_x^{(t2)} \\ \bar{u}_y^{(t2)} \\ \bar{\omega}_z^{(t2)} \end{Bmatrix}, \bar{U}_b^{(2)}\Big|_{y=h_1+h_2} = \begin{Bmatrix} \bar{u}_x^{(b2)} \\ \bar{u}_y^{(b2)} \\ \bar{\omega}_z^{(b2)} \end{Bmatrix} \tag{14}$$

$$\bar{P}_t^{(2)}\Big|_{y=h_1} = \begin{Bmatrix} \bar{\sigma}_{yx}^{(t2)} \\ \bar{\sigma}_{yy}^{(t2)} \\ \bar{m}_{yz}^{(t2)} \end{Bmatrix}, \bar{P}_b^{(2)}\Big|_{y=h_1+h_2} = \begin{Bmatrix} \bar{\sigma}_{yx}^{(b2)} \\ \bar{\sigma}_{yy}^{(b2)} \\ \bar{m}_{yz}^{(b2)} \end{Bmatrix} \tag{15}$$

where superscripts t and b denote the top and bottom boundaries of each layer, respectively.

Based on Eqs. (12)–(15), the transformed displacement vector $\bar{U}$ and traction vector $\bar{P}$ at the upper and lower boundaries of the k-th layer $(k = 1,2,3,\dots,N)$ are expressed as:

$$\begin{Bmatrix} \bar{U}_t^{(k)}\Big|_{y=0} \\ \bar{U}_b^{(k)}\Big|_{y=h_k} \end{Bmatrix} = M^{(k)}C^{(k)}, \begin{Bmatrix} \bar{P}_t^{(k)}\Big|_{y=0} \\ \bar{P}_b^{(k)}\Big|_{y=h_k} \end{Bmatrix} = N^{(k)}C^{(k)} \tag{16}$$

$$\begin{Bmatrix} \bar{U}_t^{(k+1)}\Big|_{y=h_k} \\ \bar{U}_b^{(k+1)}\Big|_{y=h_k+h_{(k+1)}} \end{Bmatrix} = M^{(k+1)}C^{(k+1)}, \begin{Bmatrix} \bar{P}_t^{(k+1)}\Big|_{y=h_k} \\ \bar{P}_b^{(k+1)}\Big|_{y=h_k+h_{(k+1)}} \end{Bmatrix} = N^{(k+1)}C^{(k+1)} \tag{17}$$

where $M^{(k)}$ and $N^{(k)}$ are 6×6 matrices depending on ζ. The top surface is traction-free. The displacement jump is imposed only at the Layer 1–Layer 2 interface, whereas the other interfaces remain perfectly bonded.

4. Solution methodology

The Fourier integral expressions are discretized using Gauss–Legendre quadrature, and the stress field is evaluated at selected points along the crack/interface line. This numerical procedure enables accurate evaluation of the stress distribution ahead of the crack tip as well as the couple-stress components. By eliminating the unknown coefficients $C_i^{(k)} (i = 1,2,3,\dots,6)$ in the governing equations, it leads to the flexibility equations for a generic layer are written as follows:

$$\bar{U} = F(\xi)\bar{P} \tag{18}$$

where $F(\xi)$ represents the flexibility matrix of the multilayered system, relating the normalized interfacial tractions $\bar{P}$ to the normalized displacement discontinuities $\bar{U}$ in the Fourier domain. Equation (19) gives the assembled flexibility matrix of the multilayer system. This matrix relates the Fourier-domain interface tractions to the corresponding displacement jumps and incorporates both classical elasticity and couple-stress contributions from each layer and the supporting substrate.

The global flexibility matrix is obtained by enforcing the boundary and interface continuity conditions at the layer boundaries. For the present multilayered configuration, it is written as [9]:

$$F(\xi)=\begin{bmatrix} F_{tt}^{(1)} & F_{tb}^{(1)} & 0 & 0 \\ F_{bt}^{(1)} & F_{bb}^{(1)}-F_{tt}^{(2)} & -F_{tb}^{(2)} & 0 \\ 0 & F_{bt}^{(2)} & F_{bb}^{(2)}-F_{tt}^{(3)} & -F_{tb}^{(3)} \\ 0 & 0 & F_{bt}^{(3)} & F_{bb}^{(3)} \end{bmatrix} \quad (19)$$

where $F(\xi)^{(k)} = M^{(k)}(N^{(k)})^{-1}$ denotes the flexibility matrix of the k-th layer. The terms F_{tt}, F_{tb}, F_{bt}, F_{bb} represent the submatrices associated with the top and bottom boundaries of each layer.

The traction-free condition at the top surface and the continuity/discontinuity conditions at the interfaces are imposed as follows:

$$\bar{P}_t^{(1)}\big|_{y=0} = \left\{\bar{\sigma}_{yx}^{(t)}, \bar{\sigma}_{yy}^{(t)}, \bar{m}_{yz}^{(t)}\right\}^T = 0 \quad (20)$$

$$\bar{U}_t^{(k+1)}\big|_{y=h_k} - \bar{U}_b^{(k)}\big|_{y=h_k} = \Delta\bar{U} = \left\{0, \Delta u_y, 0\right\}^T \quad (21)$$

$$\bar{P}_b^{(k)}\big|_{y=h_k} = \bar{P}_t^{(k+1)}\big|_{y=h_k} \quad (22)$$

$$\bar{U}^{(s)}\big|_{y=+\infty} = 0 \quad (23)$$

Within the cracked interval $-a \le x \le a$, the prescribed interfacial opening displacement Δu_y is imposed, whereas the tangential displacement component is assumed to remain zero. In addition, the micro-rotation field is assumed to be continuous across the interface. Consequently, the interfacial stresses obtained from the present formulation should be interpreted as reaction tractions required to maintain the imposed crack opening displacement.

Outside the cracked region, the interface is assumed to remain perfectly bonded, and all displacement, rotation, traction, and couple-stress quantities satisfy continuity conditions. Along the bonded interface between Layer 2 and the elastic half-plane substrate, continuity is enforced for u_x, u_y, ω_z, σ_{yx}, σ_{yy}, and m_{yz}.

The unknown traction vectors are obtained from the algebraic system derived from Eq. (18), while the coefficients $C_i^{(k)}$ $(i = 1,2,\ldots,6)$ for each layer are determined from Eqs. (16)–(17). Finally, the physical displacement, stress, and couple-stress fields in the multilayered medium are recovered through inverse Fourier transformation combined with Gauss–Legendre numerical integration.

5. Numerical results and discussion

To evaluate the reliability of the present formulation, the numerical predictions obtained from the developed solver are compared with available reference solutions reported in the literature [9]. The benchmark configuration consists of a two-dimensional elastic half-plane coated with a thin elastic layer containing a finite interfacial opening discontinuity of length $2a$, as illustrated in Figure 2. Since this benchmark problem has previously been investigated using couple-stress elasticity together with distributed dislocation formulations [9], it provides an appropriate reference for validating the current numerical implementation.

A further verification is performed by comparing the computed opening profile with the Type-I analytical displacement jump given by

$$\Delta u_y = b_0\sqrt{1-(x/a)^2}, -a \le x \le a, \quad (24)$$

where b_0 denotes the peak opening displacement at the crack center ($x = 0$).

To quantify the agreement, the relative error between the present results and the reference solution [9] was evaluated at the same normalized positions x/a used in Figure 3. The maximum and mean relative errors were approximately 1% and 0.5%, respectively. A convergence check was also performed by increasing the Fourier quadrature discretization from 79,980 to 159,980 points. The corresponding variation in the normalized stress $\sigma_{yy}/(2\mu)$ was less than 0.001%, indicating that the numerical solution is sufficiently converged for the present analysis.

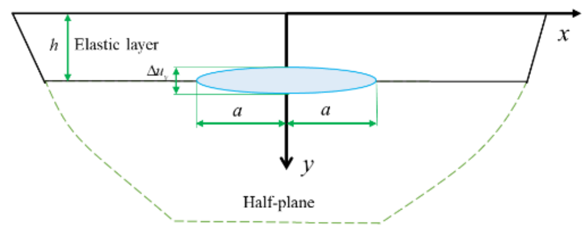

Figure 2. *Geometry of a coated elastic half-plane containing a finite interfacial opening discontinuity with total crack length* $2a$

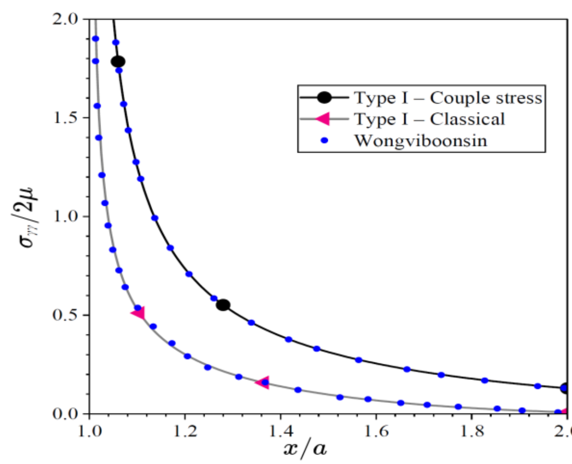

Figure 3. *Comparison of the normalized normal stress* $\sigma_{yy}/(2\mu)$ *along the interface (y = h) obtained from the present formulation and the reference solution [9]*

The numerical results are obtained using the multilayered interfacial crack model shown in Figure 1. The configuration consists of two elastic layers of equal thickness h, perfectly bonded to an elastic half-plane substrate and containing an interfacial crack of length $2a$ located at $y = h$. All materials are assumed to be homogeneous, isotropic, and governed by couple-stress elasticity. The Poisson's ratios are assumed to be identical for all regions, such that $\nu^{(1)} = \nu^{(2)} = \nu^{(s)} = 0.3$, and the characteristic material length scales are also taken to be equal, $\ell^{(1)} = \ell^{(2)} = \ell^{(s)} = 1$. The value $\nu = 0.3$ was selected as a representative Poisson's ratio for many engineering materials and is also consistent with values commonly adopted in previous couple-stress elasticity studies, thereby allowing direct comparison with available benchmark solutions [7–9]. The geometric and loading parameters are fixed at $h/a = 1$ and $b_0/a = 1$.

To investigate the influence of material mismatch, different combinations of shear moduli are considered. The notations H (hard) and S (soft) denote materials with shear modulus ratio $\mu_H/\mu_S = 2$. The material configurations considered in the present study are summarized in Table 1. Since the crack is located at the Layer 1-Layer 2 interface, the material properties of the adjacent layers directly influence the interfacial reaction stress field.

Table 1. *Material configurations used in the mismatch study* ($\mu_H/\mu_S = 2$)

Index	Layer 1	Layer 2	Half-plane substrate
HHS	Hard, μ_H	Hard, μ_H	Soft, μ_S
SHS	Soft, μ_S	Hard, μ_H	Soft, μ_S
HSS	Hard, μ_H	Soft, μ_S	Soft, μ_S

The influence of microstructural effects is examined through the normalized length-scale parameter ℓ/a, while all remaining parameters are kept constant throughout the analysis. The results are presented in terms of the normalized normal reaction stress $\sigma_{yy}/(2\mu)$ ahead of the crack tip along the interface $y = h$. Figures 4–6 show the stress distributions for the HHS, SHS, and HSS material configurations, respectively, together with the corresponding classical elasticity solution for comparison.

It is observed that the normalized normal reaction stress $\sigma_{yy}/(2\mu)$ increases sharply near the crack tip for all material configurations. For a fixed prescribed opening displacement, increasing the normalized material length-scale parameter ℓ/a leads to higher near-tip reaction stresses. This behavior indicates that couple-stress effects introduce additional microstructural resistance to local deformation and rotation near the crack tip. Consequently, larger reaction tractions are required to maintain the same prescribed interfacial opening displacement.

The material mismatch also has a significant influence on the reaction stress distribution. For the same value of ℓ/a, the SHS configuration produces the highest near-tip normalized reaction stress, followed by the HHS configuration, while the HSS configuration yields the lowest stress level. Therefore, the near-tip reaction stress follows the trend:

SHS > HHS > HSS.

For example, at $\ell/a = 1.0$ and $x/a = 1.2$, the normalized reaction stress is approximately 1.026, 0.738, and 0.515 for the SHS, HHS, and HSS configurations, respectively.

This trend indicates that the stiffness mismatch across the cracked interface strongly affects the reaction stress field. The SHS configuration produces the largest response because the crack lies between a soft upper layer and a hard lower layer, thereby generating the strongest stiffness mismatch. The HHS configuration yields a lower response because both layers adjacent to the crack are relatively stiff, whereas the HSS configuration produces the lowest response because the softer lower layer deforms more readily.

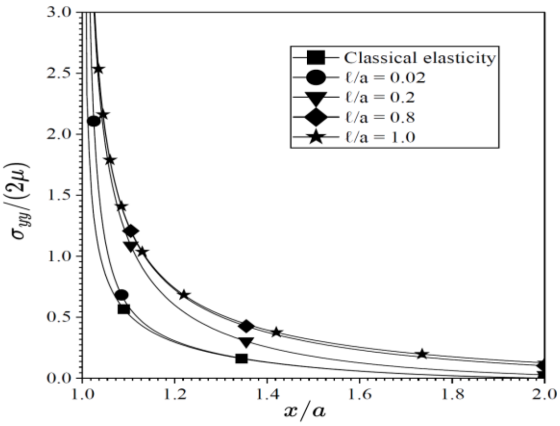

Figure 4. *Tip-side distribution of* $\sigma_{yy}/(2\mu)$ *along the interface* $y = h$ *for the HHS case with different* ℓ/a *values* ($h/a = b_0/a = 1$, $\nu = 0.3$)

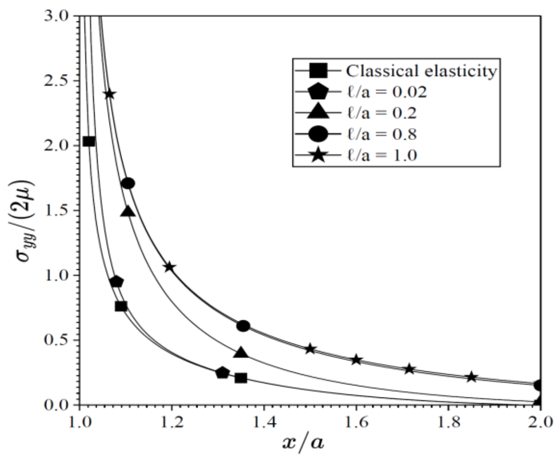

Figure 5. *Tip-side distribution of* $\sigma_{yy}/(2\mu)$ *along the interface* $y = h$ *for the SHS case with different* ℓ/a *values* ($h/a = b_0/a = 1$, $\nu = 0.3$)

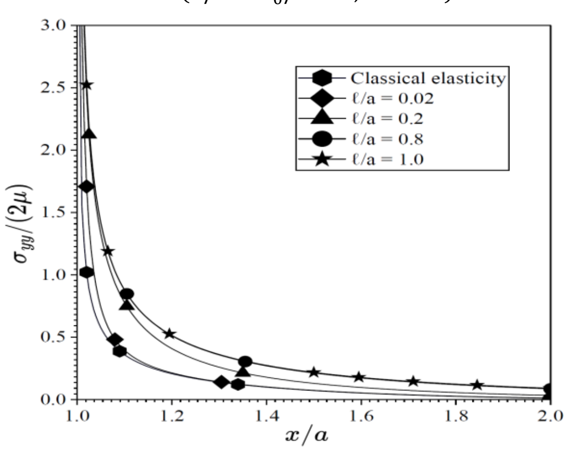

Figure 6. *Tip-side distribution of* $\sigma_{yy}/(2\mu)$ *along the interface* $y = h$ *for the HSS case with different* ℓ/a *values* ($h/a = b_0/a = 1$, $\nu = 0.3$)

From a physical perspective, the computed stress should be interpreted as a reaction stress associated with the imposed displacement discontinuity. Therefore, a higher value of $\sigma_{yy}/(2\mu)$ does not imply that a larger external traction is applied. Instead, it indicates that the material system provides stronger resistance against the prescribed crack opening displacement. This explains why the near-tip reaction stress increases as ℓ/a increases in the present displacement-controlled formulation.

6. Conclusion and remarks

This study presented a numerical formulation for analyzing a pre-existing interfacial crack in a multilayer elastic medium using couple-stress elasticity and the displacement discontinuity method (DDM). The considered configuration consists of two bonded elastic layers resting on an elastic half-plane substrate and containing a finite interfacial crack of length $2a$. Within the present displacement-controlled formulation, the prescribed crack opening displacement serves as the input condition, while the associated reaction tractions, stress fields, and couple-stress fields are obtained as part of the numerical solution. The governing equations were solved using Fourier-transform techniques combined with Gauss–Legendre numerical integration.

The numerical results demonstrated that the intrinsic material length-scale parameter has a significant influence on the near-tip mechanical response. For a prescribed crack opening displacement, increasing the length-scale parameter ℓ/a leads to higher near-tip reaction stresses, indicating that couple-stress effects introduce additional microstructural resistance to local deformation and rotation near the crack tip. Since the crack opening displacement is prescribed, the computed stress field should be interpreted as a reaction stress field necessary to maintain the imposed interfacial opening displacement, rather than as stresses generated by externally applied tractions.

The results also showed that the stiffness mismatch across the cracked interface strongly affects the reaction stress distribution. For the same prescribed crack opening displacement and the same value of ℓ/a, the near-tip normalized reaction stress follows the trend:

SHS > HHS > HSS.

The SHS configuration produced the highest reaction stress because of the strongest stiffness mismatch across the cracked interface, whereas the HSS configuration exhibited the lowest stress concentration due to the greater deformability of the softer lower layer.

Overall, the proposed formulation provides an effective framework for analyzing size-dependent interfacial fracture behavior in multilayered materials and offers a useful basis for future investigations of interfaces, functionally graded materials, and mixed-mode interfacial fracture problems.

Acknowledgments: This research was supported by Faculty of Engineering Research Fund, Thammasat University.

REFERENCES

[1] R. D. Mindlin and H. F. Tiersten, “Effects of couple stresses in linear elasticity,” *Archive for Rational Mechanics and Analysis*, vol. 11, no. 1, pp. 415–448, 1962.

[2] R. D. Mindlin, “Influence of couple stresses on stress concentrations,” *Experimental Mechanics,* vol. 3, no. 1, pp. 1–7, 1963.

[3] W. T. Koiter, “Couple stresses in the theory of elasticity,” Proceedings of the Koninklijke Nederlandse Akademie van Wetenschappen, Series B, vol. 67, pp. 17–44, 1964.

[4] P. A. Gourgiotis and H. G. Georgiadis, “Distributed dislocation approach for cracks in couple-stress elasticity: shear modes,” *International Journal of Fracture,* vol. 147, no. 1, pp. 83–102, 2007. doi:10.1007/s10704-007-9156-9.

[5] H. G. Georgiadis and P. A. Gourgiotis, “An approach based on integral equations for crack problems in standard couple-stress elasticity,” in *Mechanics of Generalized Continua: One Hundred Years After the Cosserats*, G. A. Maugin and A. V. Metrikine, Eds. New York: Springer, 2010, pp. 253–262.

[6] P. A. Gourgiotis and H. G. Georgiadis, “The problem of sharp notch in couple-stress elasticity,” *International Journal of Solids and Structures,* vol. 46, no. 13, pp. 2630–2641, 2009. doi:10.1016/j.ijsolstr.2009.02.013.

[7] W. Wongviboonsin, P. A. Gourgiotis, V. C. Nguyen, and S. Limkatanyu, “Size effects in two-dimensional layered materials modeled by couple-stress elasticity,” *Frontiers of Structural and Civil Engineering,* vol. 15, no. 2, pp. 425–443, 2021. doi:10.1007/s11709-021-0707-y.

[8] W. Wongviboonsin, T. M. Le, J. Lawongkerd, P. A. Gourgiotis, and J. Rungamornrat, “Microstructural effects on the response of a multilayered elastic substrate,” *International Journal of Solids and Structures,* vol. 241, 111480, 2022.

[9] W. Wongviboonsin, P. A. Gourgiotis, and J. Rungamornrat, “Interfacial displacement discontinuity in coated substrate with couple-stress effects,” *in Proceedings of the 17th East Asia-Pacific Conference on Structural Engineering and Construction (EASEC-17), Singapore*, 2022, pp. 843–851.

[10] I. N. Sneddon, *Fourier Transforms*. New York: McGraw-Hill, 1951.